Composites: Part A 182 (2024) 108164

Contents lists available at ScienceDirect

Composites Part A

journal homepage: www.elsevier.com/locate/compositesa

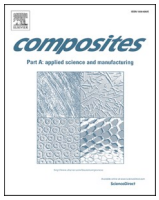

Bicontinuous silica-epoxy nanocomposites by aerogel infusion

Charles M.D. Shaw [a], David B. Anthony [b], Ian Hamerton [c], Milo S.P. Shaffer [a,b,*]

[a] Department of Materials, Imperial College London, South Kensington Campus, London SW7 2AZ, UK
[b] Department of Chemistry, Molecular Sciences Research Hub (MSRH), Imperial College London, 82 Wood Lane, London W12 0BZ, UK
[c] Bristol Composites Institute, School of Civil, Aerospace, and Design Engineering, Faculty of Science and Engineering, University of Bristol, Queen's Building, University Walk, Bristol BS8 1TR, UK

ARTICLE INFO

Keyword:
Aerogel
3-Dimensional reinforcement
Bicontinuous network
Nanocomposite

ABSTRACT

Interpenetrated, bicontinuous nanocomposites are formed by fully infusing monolithic mesoporous silica (silica aerogel) with epoxy resin. The long-range connectivity of the silica network facilitates direct load transfer and enforces sample homogeneity. The silica networks are prepared using sol–gel chemistry, informed by new phase diagrams, adapted to maximise reinforcement content in the subsequent bicontinuous composite. The infusibility of the aerogels is correlated to pore characteristics determined by gas sorption, as a function of silica aerogel density. Silica reinforcement loadings of up to 22 silica vol.% are fully consolidated, with only a modest reduction in glass transition temperature and no change in cure conditions. The reinforcement improves both hardness (+23 %) and reduced modulus (+17 %) of the baseline resin. These properties increase with aerogel content *via* a power law relationship which demonstrates the direct role of the connected silica phase as a reinforcing network and motivates future studies to extend the applicable range.

1. Introduction

Polymer nanocomposites exploit inorganic nanoparticles to increase stiffness, via direct reinforcement [1], and toughness, by introducing a variety of additional energy absorption mechanisms [2]. This approach has been widely explored in a range of matrices, including the epoxy systems commonly applied in high performance fibre composites. The nanoreinforcement usually consists of discrete (discontinuous) particles, dispersed in the resin at modest loading fractions; the enhancement is typically limited by particle agglomeration at higher weight loadings which form stress concentrators, and by self-filtration, or other processing issues, in fibre composite matrix applications [3,4]. *In situ* synthesis of inorganic particles within the liquid resin precursor can mitigate agglomeration issues [1]; the commercial NANOPOX® range (Evonik, Essen, DE) uses this approach to provide up to 40 wt.% predispersed nanosilica in epoxy resin (decreased to approximately 34 wt.% after mixing with amine hardener); the degree of reinforcement is more pronounced (30 % increase in compression modulus at 25 wt.% silica loading) than for *ex-situ* formed silica nanoreinforcements [5], although high viscosity may still necessitate dilution to allow effective infusion, in practice [6]. This paper develops an alternative strategy, hypothesising that a continuous 3D nanostructured skeleton (Fig. 1 (a)) may provide improved long-range load transfer compared with discontinuous particulate reinforcements. When infused with epoxy resin, this stiff continuous inorganic reinforcement should form a bicontinuous network with the organic component (Fig. 1 (d)), combining the complementary properties of the two phases in an interlocking structure. Bicontinuous nanocomposite structures are found in Nature where high stiffness/hardness and toughness are needed. For example, the dactyl club of the mantis shrimp contains an interpenetrating inorganic–organic coating that provides sufficient toughness to prevent catastrophic failure when rapidly striking mollusc shells [7]. Synthetic bicontinuous materials are commonly formed by an induced phase separation of a liquid precursor to give two interlocking phases. Examples include soft, organic multifunctional bijels (bicontinuous interfacially jammed emulsion gels) formed by polymerisation induced phase separation [8] and bicontinuous metal systems formed through molten salt dealloying [9]. Recently, a bicontinuous organic–inorganic nanocomposite has been formed by polymerisation of an organic–inorganic monomer [10]. The organic and inorganic phases of this substance are interpenetrating at the length-scale of several nanometres leading to a material which exhibits the high stiffness of a ceramic with the elasticity

* Corresponding author at: Department of Materials, Imperial College London, South Kensington Campus, London SW7 2AZ, UK.
E-mail addresses: c.shaw20@imperial.ac.uk (C.M.D. Shaw), d.anthony08@imperial.ac.uk (D.B. Anthony), ian.hamerton@bristol.ac.uk (I. Hamerton), m.shaffer@imperial.ac.uk (M.S.P. Shaffer).

https://doi.org/10.1016/j.compositesa.2024.108164
Received 15 December 2023; Received in revised form 18 March 2024; Accepted 19 March 2024
Available online 21 March 2024

of a rubber. However, the required hot-pressing step (120 °C, 110 MPa) may hinder formation of large components. For structural composite applications, bicontinuous constituents with high mechanical performance and good processability are required. In this work, a bicontinuous nanocomposite is proposed consisting of a stiff continuous silica reinforcement interlocked with a commercial structural epoxy resin. In previous examples of silica-epoxy systems, liquid–liquid precursors tend to form only small clusters or nanoparticles (Fig. 1 (c)), rather than long-range connected structures [11]. Instead, silica-epoxy bicontinuous networks can be accessed by pre-forming monolithic mesoporous silica (silica aerogel) before backfilling the porous structure with epoxy resin. Pre-forming a uniform silica network precludes unwanted heterogeneous particulate agglomeration even at high weight loadings, hence a fully connected evenly-dispersed 3D reinforcement is possible. The use of silica aerogel as a powdered filler is typically limited to loadings of <5 wt.% for reasons of agglomeration and packing efficiency [12]. Previous use of organic polymers to reinforce silica aerogel networks has used low concentrations of epoxy monomers dissolved in solution to crosslink the primary silica particles to give an "X-aerogel". In such materials, pore backfilling is minimised in order to retain the low density, and hence thermal conductivity, of the original aerogel, whilst reducing its fragility (Fig. 1 (b)) [13]. The goal in the present work is quite different: a vacuum infusion procedure was designed to fill the entire pore volume giving a two-phase silica-epoxy bicontinuous network (Fig. 1 (d)) such that the silica acts as a continuous reinforcement for the epoxy matrix. Vacuum backfilling of silica aerogel with soft electrolyte has recently been reported for battery applications, although the infused phase serves no structural role [14]. A vacuum infusion method has also been used to produce a silica-epoxy bicontinuous network as matrix for woven glass fibre composite. This additional reinforcement yielded a 27 % improvement in both compression modulus and interlaminar shear strength when compared to baseline samples with a conventional epoxy resin matrix [15]. In this hierarchical composite, the continuous silica matrix reinforcement likely limited the onset of failure through kink-band formation by providing lateral support between the fibres. However, the study was only a proof of concept; there is great potential for improvement since neither the infusion process, nor the properties of the isolated nanocomposites were studied.

In this work, an ambient temperature sol–gel procedure was developed to form monolithic bicontinuous nanocomposites with well-defined geometry at the centimetre scale. The chemistry for the reinforcing network is similar to typical silica aerogel syntheses [16], however, the goal was to maximise envelope density whilst retaining a sufficiently open pore structure to facilitate high silica loadings in the resulting bicontinuous nanocomposite. This aim contrasts with typical aerogel literature where ultra-low density is sought for lightweight thermal insulation [17]. A sol–gel synthesis was selected as the source of mesoporous silica due to the mild chemistry (neutral pH or mildly acidic/basic) and temperatures (typically room temperature) involved. These conditions are amenable to combination with fibrous reinforcements which may degrade in the presence of highly acidic or basic conditions (glass fibre) or high temperature (carbon fibre) [18,19]. To avoid local instabilities, the length scale of the bicontinuous structure should be significantly shorter than the diameters (5 μm–10 μm) of the reinforcing fibres with which it will be combined. Consequently, additive manufacturing techniques are not generally applicable, here, due to insufficient resolution, low production rate, and the complexity of future combination with fibre reinforcement [20]. In sol–gel synthesis, the ultimate factor determining the maximum silica envelope density (without loss of porosity) is the volume fraction of orthosilicate in the sol–gel reaction volume. In turn, this volume fraction is limited by the miscibility of the orthosilicate with the water required for hydrolysis. For this reason, miscibility experiments were carried out with various orthosilicates, organic solvents and water to determine the most suitable reagent ratios. A new procedure was also needed to produce dense bicontinuous nanocomposite specimens for property determination.

2. Results and discussion

2.1. Maximising density of monolithic mesoporous silica

Silica aerogel may be formed by hydrolysis of an orthosilicate

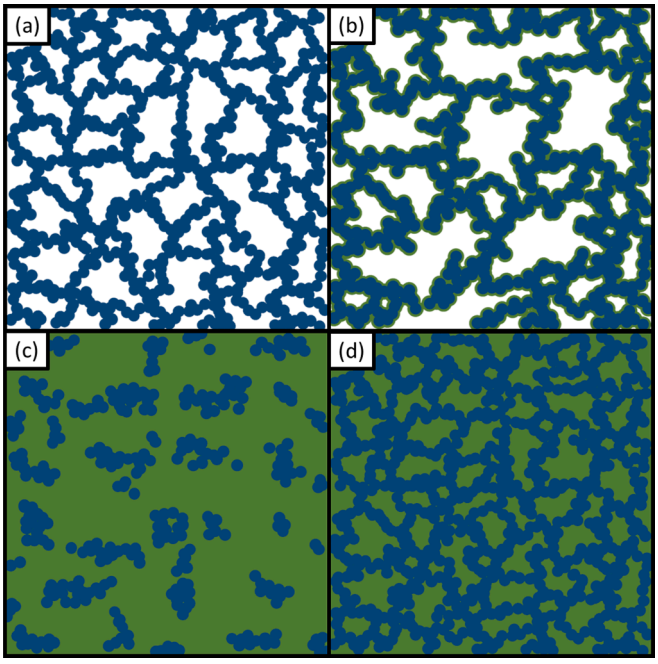

Fig. 1. Schematic cross-sectional representations of structures combining silica aerogel (dark blue) and epoxy resin (dark green). (a) Low density monolithic silica aerogel. (b) Monolithic X-aerogel formed by crosslinking silica aerogel with epoxy resin [13]. (c) Powdered silica aerogel dispersed in epoxy resin [12]. (d) Bicontinuous silica-epoxy nanocomposite presented in this work. (For interpretation of the references to colour in this figure legend, the reader is referred to the web version of this article.)

precursor ($(Si(OR)_4)$, where R = alkyl residue) followed by condensation to form a wet gel which is then dried. Tetraethylorthosilicate (TEOS) is commonly used in silica aerogel synthesis due to its low cost and relatively low rates of reaction which facilitate easier kinetic control over reaction processes. The use of tetramethylorthosilicate (TMOS) is occasionally reported but, due to the decreased steric bulk of methoxy over ethoxy, it exhibits faster rates of hydrolysis, limiting kinetic control [21]. The miscibilities of TMOS and TEOS with water and ethanol were measured to determine the maximum accessible concentration of orthosilicate for each precursor. The resulting ternary miscibility plots (Fig. 2 (a)) show that TEOS requires a polar organic solvent (ethanol) to form a single-phase mixture with water. Surprisingly, there appears to be only one example of a ternary phase diagram for this important system in the literature; the limited data from 1946 agree with the new results [22], although there is a small offset attributed to the greater purity of alcohol in the present study. In contrast, TMOS was found to have effectively unlimited miscibility with water. Although a phase boundary was observed on initial mixing, it disappeared within one hour. This miscibility is attributed to the rapid evolution of methanol, through reaction between initially unmixed TMOS and water phases at the liquid–liquid interface, that solubilises the two phases without the need for explicitly added solvent. For TMOS, the maximum silica content in the resulting gel is therefore limited only by the requirement for a minimum 2:1 M ratio of H_2O to orthosilicate for complete gelation [23]. TEOS, on the other hand, requires the addition of organic solvent (which dilutes the reaction, decreasing the TEOS concentration) to form a single phase before reaction can occur [21]. It is, therefore, in principle possible to form a sol with 74 % higher orthosilicate mole fraction (χ_{max}) from TMOS than TEOS (TMOS: $\chi_{max} = 0.33$, TEOS: $\chi_{max} = 0.19$) (Fig. 2 (b)). Hydrolysis of TMOS to acidic $Si(OH)_n(OMe)_{4-n}$ reduces the pH from 6.5 to 4, where the sum of the rates of hydrolysis and gelation is a maximum (Fig. S1 (a)) [24]. Consequently, gelation occurs without the need for any additional catalysts or elevated temperature. Furthermore, silica aerogel formed under initially neutral conditions has been found to have superior mechanical properties to those formed under basic conditions due to the more reticulated structure of the former [25]. Gels were prepared from TMOS – H_2O mixtures across a wide range of TMOS volume fractions ($\varphi_{TMOS} = 0.09$–0.67), with gelation times ranging from 5 h 50 min ($\varphi_{TMOS} = 0.67$) to 11 h 45 min ($\varphi_{TMOS} = 0.09$), at 25 °C (Fig. S1 (b)). Gelation times on the scale of several hours are convenient for processing of both monolithic and composite samples.

2.2. Silica aerogel monoliths

These TMOS – water mixtures ($\varphi_{TMOS} = 0.09$ - $\varphi_{TMOS} = 0.67$) were used to form silica aerogel monoliths across a range of densities, in order to determine their physical properties and potential for epoxy infusion. A cylindrical geometry (diameter ≈ 6 mm, length ≈ 18 mm) was selected to enable lathing of the subsequent bicontinuous nanocomposite to produce smooth parallel faces for microindentation measurements. Monoliths were prepared by stirring the appropriate mixture of TMOS and water for 3 h at 25 °C before transfer of the liquid sol to high density polyethylene moulds. After gelation, samples were aged in the supernatant for 4 days at room temperature to consolidate the silica network through increased inter-particle crosslinking. Samples were subsequently demoulded and transferred to ethanol. Ethanol was exchanged three further times before hydrophobisation of the silica surface was performed by immersion of the wet gels in a trimethylchlorosilane (TMCS):*n*-hexane:ethanol mixture (1:1:8 ratio by volume) for 4 days at 25 °C. Samples were exchanged first to ethanol and then acetone before drying. Samples were dried from supercritical CO_2 to minimise the capillary forces that drive pore collapse and overall sample shrinkage. A more detailed description of this synthesis may be found in the electronic supporting information (ESI). The success of the TMCS treatment was confirmed by infrared spectroscopy; the untreated aerogel shows a broad infra-red signal centred at 3000 cm^{-1} indicating significant water absorption that is absent for the treated sample (Fig. S2 (a,b)). The hydrophobicity resists pore collapse, through a "spring back" effect, that stabilises the dried specimen leading to a uniform, uncracked monolith (Fig. S2 (c)) [26]. Specimens were nonetheless dried under supercritical conditions as ambient pressure drying to TMOS-derived aerogels is known to result in sample disintegration even with a hydrophobic surface [27]. Untreated samples were found to rapidly disintegrate due to the capillary pressure associated with the absorption of atmospheric moisture (Fig. S2 (d)). In the current context, the inert hydrophobic surface also avoids the need to remove absorbed atmospheric water prior to epoxy infusion and the need to adjust the epoxy-hardener stoichiometry. Dried samples were characterised for envelope density, skeletal density, porosity, pore radius, and specific surface area (SSA) by gas adsorption (Table S1). Envelope density (ρ_b) was found to increase linearly with increasing φ_{TMOS} (Fig. 2 (c)). These densities are a close match for predicted values after accounting for the mass contribution of the trimethylsilyl (TMS) functionalisation and the measured shrinkage. The mass of surface TMS groups in each aerogel monolith was estimated by combining SSA data (Brunauer-Emmett-Teller (BET) analysis) with TMS areal density reported in literature (3.5 molecules. nm^{-2}) [28]. Independent of envelope density, the treated aerogel is consistently around 70 wt.% SiO_2 and 30 wt.% TMS coating. Surface area increased from 878 $m^2.g^{-1}$ at $\varphi_{TMOS} = 0.09$ to 1030 $m^2.g^{-1}$ at $\varphi_{TMOS} = 0.50$ before decreasing to 888 $m^2.g^{-1}$ at $\varphi_{TMOS} = 0.67$ (Fig. 2 (e)) (Fig. S3). Across this same range, mean pore radii decrease from 3.8 nm to 1.7 nm (Fig. 2 (e,f)), reflecting the decrease in gelation time observed with increasing TMOS concentration (Fig. S1 (b)), and the higher volume fraction. At higher rates of gelation (shorter gelation time), nucleation of new particles is expected to outpace the growth of existing particles thus favouring the formation of a greater number of (on average) smaller particles [29]. These smaller particles pack more closely and have larger surface area to volume ratios resulting in a structure with smaller average pore sizes and higher surface areas. The decrease in SSA between $\varphi_{TMOS} = 0.50$ and $\varphi_{TMOS} = 0.67$ is attributed to the formation of micropores not measurable by N_2 isotherm, which may also be the origin of the plateau in mean pore radius above $\varphi_{TMOS} = 0.50$.

The envelope densities are affected by sample shrinkage (Fig. 2 (d)), mostly during the drying step. However, there is also a fundamental 'shrinkage' that occurs prior to drying due to the non-ideal mixing of the precursor components and the subsequent condensation reaction, as shown in the ESI (Fig. S4). Overall shrinkage of dried samples decreases sharply above $\varphi_{TMOS} = 0.33$. This finding is attributed to the stiffer silica network formed at higher silica aerogel densities [30], and results in a non-linear relationship between φ_{TMOS} and ρ_b at high φ_{TMOS} (Fig. 2 (c)). The aerogel density (ρ_b) is directly proportional to the silica vol.% (1 - Φ) via the porosity (Φ) (Equation S2); volume fraction is the more appropriate variable when considering infused composites.

2.3. Infusion of silica aerogel monoliths with epoxy resin

Vacuum infusion was used to fill the silica network of aerogel specimens formed in Section 2.2 (Fig. 1 (a), Fig. 3 (a)) with epoxy resin, to form a bicontinuous composite (Fig. 1 (d)). Epoxy resin was infused into the cylindrical mesoporous silica monoliths by immersion in degassed low viscosity Gurit Prime 27 epoxy resin – Extra Slow Hardener mix, under reduced pressure (1 mbar) for 6 h at 22.5 °C. This temperature balances decreased resin viscosity at higher temperature and decreased cure time at lower temperature. As the hydrophobised silica surface is chemically inert, it was not necessary to modify the resin:hardener ratio. The progress of infusion was observed through the evolution of bubbles as the epoxy resin displaces remaining air in the pores and by increased transparency, as the loss of refractive index contrast reduces the Rayleigh scattering that gives silica aerogel its characteristic blue hue. Following infusion, samples were cured at 25 °C for a further 18 h before post curing at 50 °C for 16 h in accordance with the recommended cure schedule. Fully infused samples retained their

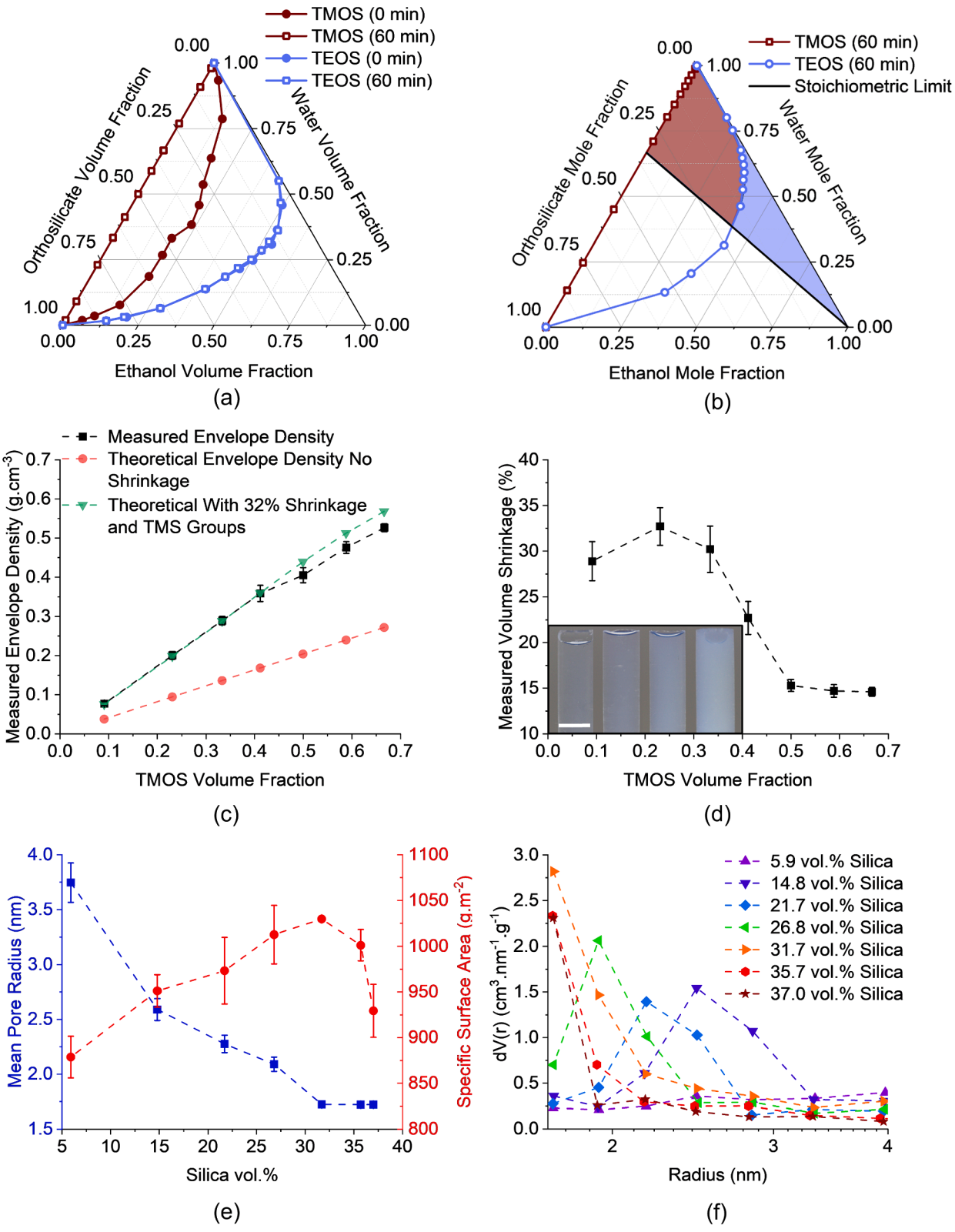

Fig. 2. (a) Ternary phase diagrams showing the miscibility, plotted in units of unmixed volume fraction, for TMOS and TEOS in water and ethanol at 0 min and 60 min after combination. Mixtures are immiscible to the left and miscible to the right of each boundary line. Measured changes in volume after mixing are shown in Fig. S3. (b) Ternary phase diagrams showing miscibility, plotted in units of mole fraction, for TMOS and TEOS at 60 min after mixing. Black line indicates minimum 2:1 stoichiometry of H_2O:TMOS required for gel formation. Maroon and blue shaded regions show suitable reagent combinations for gel formation from TEOS and TMOS, respectively. (c) Plot of silica aerogel envelope density for monoliths of increasing precursor TMOS volume fraction, alongside plots for theoretical density of silica aerogel samples formed from these precursors accounting for surface treatment and shrinkage. (d) Main: Volume shrinkage of cylindrical silica aerogel monoliths as a percentage decrease in volume. Insert: Photographs of silica aerogel monoliths of decreasing envelope density from left to right: 0.527 $g{\cdot}cm^{-3}$, 0.359 $g{\cdot}cm^{-3}$, 0.289 $g{\cdot}cm^{-3}$ and 0.201 $g{\cdot}cm^{-3}$, scale = 5 mm. (e) Mean pore radius (BJH) and specific surface (BET) plotted for silica aerogel with increasing silica vol.%. (f) Pore radius distributions (BJH) for silica aerogel monoliths synthesised from various silica vol.%. For (c), (d) and (e) bars show one standard error.

cylindrical geometry with no further shrinkage (photographs, Fig. 3 (b)); the change of morphology from an open porous network to a void-free solid was observed by scanning electron microscopy (SEM) (Fig. 3 (c, d)). The success of backfilling was quantified in terms of backfilling efficiency (β) according to Equation 1,

$$\beta = \frac{\Delta\rho_b}{\Phi.\rho_e} \quad (1)$$

where $\Delta\rho_b$ is the difference in envelope density between the silica aerogel monolith and the epoxy-infused silica aerogel monolith, Φ is the porosity of the silica aerogel monolith, and ρ_e is the cured epoxy resin density determined by Archimedes' balance method. β ranges from 0 to 1, with $\beta = 1$ indicating complete backfilling of aerogel pores with epoxy resin and $\beta = 0$ indicating no backfilling. Across the range of aerogels (5.9 silica vol.% to 37.0 silica vol.%), the backfill efficiency, β, shows

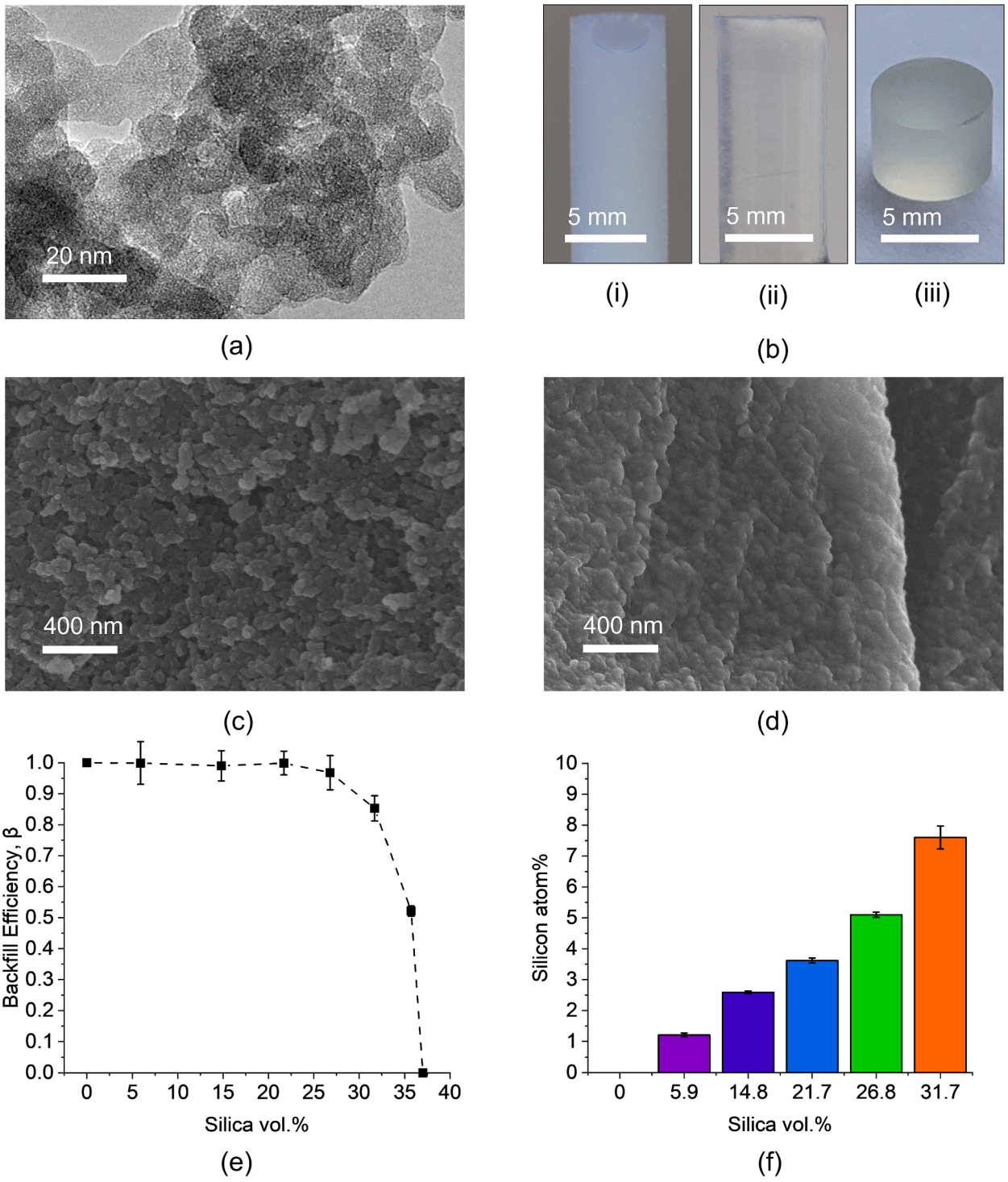

Fig. 3. (a) TEM micrograph of silica aerogel (21.7 silica vol.%). (b) Photographs of silica aerogel (i) before epoxy infusion (ii) after epoxy infusion (iii) after machining to microindentation specimen geometry. (c) SEM of silica aerogel fracture surface (21.7 silica vol.%). (d) SEM of silica-epoxy bicontinuous nanocomposite fracture surface (21.7 silica vol.%). (e) Backfill efficiency plotted against silica vol.% for silica aerogel infused with epoxy resin. (f) Elemental composition (silicon atom%) of silica-epoxy bicontinuous nanocomposites formed from aerogels of different silica volume fraction. For (e) and (f) bars show one standard error.

consistently full infusion for lower silica volume fractions (Fig. S5 (a)), dropping off dramatically above around 25 silica vol.% (Fig. 3 (e)). Partly infused samples showed opaque regions due to diffraction at the air-epoxy interfaces within the porous structure (Fig. S5 (b)) and cracking of the sample was observed at the highest silica content (Fig. S5 (c)). Since the Barrett-Joyner-Halenda (BJH) pore radius distributions are narrow and unimodal for $\varphi_{TMOS} > 0.2$ (Fig. 2 (f)), the behaviour can be attributed to a minimum pore radius of approximately 2 nm for complete backfilling of mesoporous silica with epoxy resin (Fig. 2 (e)).

Statistical elemental analysis by SEM energy dispersive X-ray analysis (Fig. 3 (f)) (25 independent point spectra spaced at 10 μm in a 5 x 5 grid, on three separate pieces of each sample) confirmed a uniform distribution of silica in the bicontinuous network. Absolute silica contents are a good match to those calculated from density measurements for all samples, except for a deviation at 31.7 silica vol.% due to the low backfill efficiency ($\beta = 0.85$) (Fig. S6).

2.4. Thermal analysis of bicontinuous nanocomposite

Nanocomposite polymer matrices often have significantly different glass transitions to the bulk resin, due to the large interfacial area, which can either increase or decrease free volume depending on the strength of the intermolecular interactions [31]. The glass transition temperature (T_g) was initially measured by differential scanning calorimetry (DSC, −50 °C to 150 °C) after the recommended epoxy post cure (50 °C) (Fig. 4 (a)). The T_g of unreinforced epoxy resin (67.5 °C) reduces slightly with increasing silica content, up to 26.8 silica vol.%, as expected on introducing an increasing fraction of inert (methylated) interface; the lack of covalent interaction is expected to increase free volume and reduce the average cross-link density. The partial reversal of the trend at 31.7 silica vol.% may be an artefact of lower thermal conductivity of the sample as voidage increases. A similar trend is observed on a second DSC heating cycle, but with a higher absolute T_g, due to additional curing during the first cycle heating to 150 °C. The small reductions in T_g are not practically significant; although they may indicate a weak interface, stress transfer in the bicontinuous system likely relies predominantly on mechanical keying between the rough interpenetrated structures. In the future, nanocomposite performance might be improved by developing a covalent silica-epoxy interface to increase load transfer and introduce more debonding toughening as has been reported for particulate reinforcements [31]. However, the complexity of altering the resin-hardener stoichiometry would have to be considered. Across the

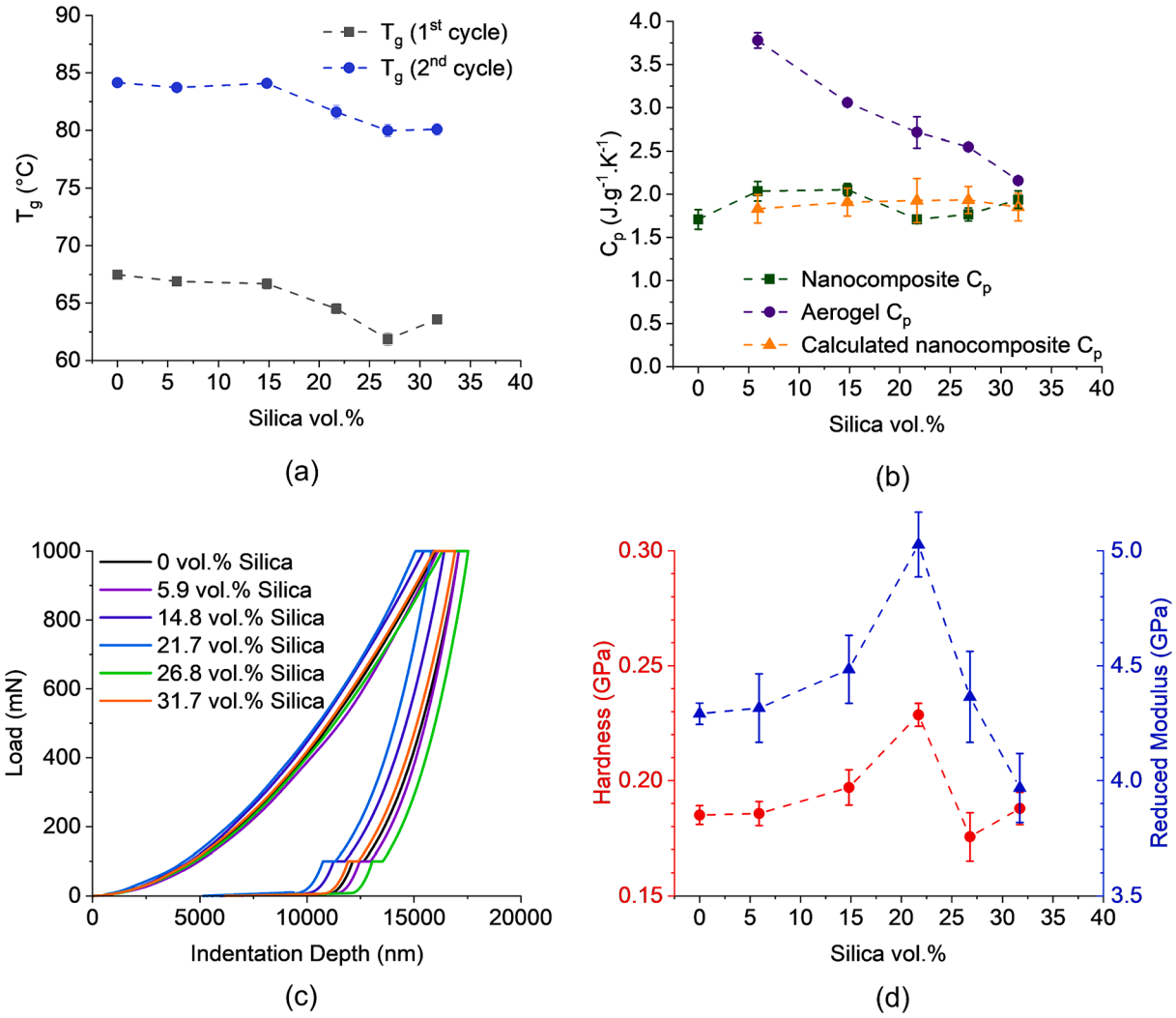

Fig. 4. (a) DSC-determined T_g plotted against silica vol.% for bicontinuous nanocomposites (1st and 2nd heating cycles shown). (b) C_p plotted against silica vol.% for bicontinuous nanocomposites, silica aerogels and predictions for the nanocomposites based on a rule of mixtures combination of epoxy resin and aerogel heat capacities. (c) Representative depth-load hysteresis plots for microindentation (1000 mN load) for silica-epoxy bicontinuous nanocomposites of various silica loadings (silica vol.%). (d) Microindentation hardness and reduced modulus (1000 mN load) plotted against silica vol.% for silica-epoxy bicontinuous nanocomposites and pure epoxy baseline (0 silica vol.%).

current aerogel monolith samples, heat capacity decreases with increasing density. This relationship is attributed to the decreased mobility of the surface TMS groups with decreasing aerogel pore size; the much higher absolute heat capacities (2 $J{\cdot}g^{-1}{\cdot}K^{-1}$–4 $J{\cdot}g^{-1}{\cdot}K^{-1}$) than for amorphous silica (0.70 $J{\cdot}g^{-1}{\cdot}K^{-1}$) suggest that these surface bound groups contribute significantly [32]. However, the heat capacity of the bicontinuous nanocomposite is relatively independent of silica loading, consistent with a simple rule of mixtures estimate (Fig. 4 (b)).

2.5. Micromechanical characterisation of bicontinuous Silica-Epoxy nanocomposites

Mechanical properties of the cured nanocomposites were measured by indentation, on cylindrical samples (Section 2.3) lathed & then wet-polished to form parallel sided disks (diameter ≈ 6 mm, length ≈ 4 mm–6 mm). A 1000 mN load was chosen because conversion of the measured reduced modulus of the unreinforced epoxy resin at this load (4.3 GPa) to an elastic modulus with Equation S7 (ESI) gave a value of 3.6 GPa. This result is in close agreement to the known macroscopic elastic modulus of this resin (3.5 GPa) [33]. A 1000 mN load was also used for previous nanoreinforced epoxy resin studies [34]. Representative depth-load plots are given in Fig. 4 (c). Hardness and reduced modulus were calculated from these plots using the Oliver and Pharr method [35]. The hardness and reduced modulus of the baseline resin increase monotonically, though non-linearly, on increasing silica loading up to 21.7 silica vol.% (Fig. 4 (d)). This response is qualitatively similar to trends seen in literature for the mechanical properties of uninfused, monolithic silica aerogel samples where both compression modulus and compressive strength are related to the silica content (envelope density) by a power law relationship of the form $y \propto \rho_b^m$ [25,30]. Herein the exponents, m, are referred to as α (reduced modulus, E_R) and γ (hardness, H). For fully infused silica-epoxy bicontinuous networks (up to 21.7 vol% silica), fitting of hardness and reduced modulus against precursor aerogel envelope density (Table S1, Table S4) give the following power law relationships:

$$E_R = 4.3 + 102\rho_b^{3.9} \quad (1)$$

$$H = 0.19 + 4.0\rho_b^{3.7} \quad (2)$$

The exponent for the nanocomposite elastic modulus power law (α = 3.9) is a good match for that reported in literature (α = 3.8) for uninfused TMOS-derived silica aerogel prepared under initially neutral conditions; more generally, α falls in the range $3 < \alpha < 4$ for silica aerogel. These values originate in the fractal nature of the aerogel network which gives increased connectivity with increasing density leading to a greater proportion of the network being load bearing [36]. In contrast, for more ordered open cell foams an exponent value of α = 2 would be expected. The exponent for the hardness response of the silica-epoxy bicontinuous nanocomposite (γ = 3.7) indicates a similar fractal network response to the modulus. Whilst there are many reported values of α in literature, for pure aerogel monoliths, the only value for the hardness exponent (γ = 2.0) is significantly lower than for the nanocomposite [37]. One possible explanation is that the elastic response relates to silica network structure in a similar way for both aerogel and infused nanocomposite (similar α), but hardness shows a different behaviour for porous monoliths (lower γ) due to crushing. For the dense nanocomposite, the silica network can continue to contribute mechanically even after it begins to fragment. In any case, the power law relationships between nanocomposite silica content and mechanical properties indicate that the long-range connectivity of the fractal silica network remains intact following epoxy backfilling, consistent with the formation of bicontinuous, mutually-interpenetrating phases, and providing good evidence of direct and effective reinforcement. The maximum hardness (0.22 GPa) and reduced modulus (5.03 GPa) are 23 % and 17 % higher than the baseline epoxy, respectively; the overall density increase is only 4.0 %. In principle, it would be interesting to compare an equivalent discontinuous system to the bicontinuous nanocomposites. However, grinding the porous aerogel to a powder reduced the maximum silica loading to around 10 wt.%, as packing efficiency was degraded. Denser silica particles could pack more efficiently, but most nanocomposite examples suffer agglomeration for loadings above 5–10 wt.%. The state-of-the-art *in-situ* dispersed silica (Nanopox) system can maintain a relatively good dispersion and an apparently linear increase in both indentation and compressive moduli up to ~15 wt.% [385]. This highly developed commercial nanocomposite resin shows a better performance in this loading range than the prototype bicontinuous network (see Fig. S8), most likely due to optimised covalent bonding at the silica-epoxy interface which enhances inter-phase load transfer. Detailed studies on *ex-situ* silica particles have shown that a covalent silica epoxy interface improves nanocomposite strength, modulus and toughness [31]. Nanopox composites have been modelled in compression by Halpin-Tsai and Lewis-Nielsen approaches which predict a super-linear relationship between filler content and elastic modulus, but the experimental data fail to match the predicted super-linear behaviour at higher loadings, as attributed to poor adhesion or agglomeration [5]. Other Nanopox studies show a sub linear behaviour, as frequently observed in a wide range of nanocomposites [39,40]. The power law response of the bicontinuous network is, therefore, strikingly different to both typical ex-situ silica particle and in situ Nanopox nanocomposites, confirming the different connectivity [1]. Based on the power laws, void-free backfilling of higher density aerogels (>30 silica vol.%) is projected to offer significant further increases in mechanical performance with reduced moduli well in excess of 6 GPa (Fig. S8). However, at higher silica loading (>25 %), incomplete infusion (Fig. S5) currently leads to declining properties. Successful epoxy-infusion of such high-density aerogels may be enabled, in the future, by lower resin viscosity resins and longer working times, alongside better control of aerogel porosity to increase pore size and connectivity. Additionally, the use of a silica aerogel bearing reactive surface groups may bring dual benefits of increased epoxy wetting (for improved backfilling) and a covalent silica-epoxy interface (for improved mechanical performance).

3. Conclusion

In summary, new monolithic bicontinuous silica-epoxy nanocomposites have been prepared, characterised, and evaluated mechanically. Unlike typical aerogel syntheses, here, high aerogel densities are designed to maximise the inorganic content in the final composites; ternary phase diagrams help to identify the highest usable concentrations of precursors in given solvents. To form nanocomposite samples, the silica network was infused with low viscosity epoxy resin; a minimum pore radius greater than 2 nm was suitable for complete backfilling, with void content below 1 vol%. Fully infused samples were obtained at up to 21.7 silica vol.%. Scanning electron microscopy showed good epoxy-silica wetting, no evidence of voids and, by elemental analysis, uniform silica distribution. The original shape of the silica aerogel monolith is maintained during this infusion, indicating that the network of interparticle linkages remains intact. Instrumented microindentation measurements show a power law increase in both material hardness and reduced modulus for fully consolidated bicontinuous samples. The trend is similar to the responses of aerogel monoliths reported in the literature but with higher absolute values at equivalent silica volumetric content. This finding further evidences the connectivity of the silica network in the nanocomposite and contrasts with the linear (or sub-linear) relationships between filler content and mechanical properties seen for particulate reinforced systems [5]. Compared to typical nanoparticulate systems, the infusion process ensures a homogeneous micro(nano)structure even at high loadings, whilst the bicontinuous connectivity enables different load transfer mechanisms. The power law response indicates significant benefits if the

system can be extended to higher silica contents. There is great scope for further exploration, including varying pore size, network architecture, and material combinations. In addition, developing a covalent interface between the phases should deliver further improvements in mechanical performance. These nanocomposite resin systems can be combined with conventional fibre reinforcements for polymer matrix composites, in order to address matrix-dominated failures. For example, when loaded in uniaxial compression, the long-range connectivity of the silica network in the bicontinuous nanocomposite should improve load transfer between fibres leading to increased microbuckling resistance. By delaying the onset kink band formation, bulk composite compressive strength should be improved. Future work will investigate the relevant bulk mechanical properties of bicontinuous silica epoxy nanocomposites and the synthesis and mechanical properties of silica epoxy bicontinuous nanocomposites combined with continuous ordered carbon and/or glass fibre reinforcement. Scaling of aerogel synthesis for production of practical components will be a key challenge. However, ambient pressure drying techniques can maintain the long-range silica network connectivity without the need for costly supercritical drying, when fibre reinforcements are included. The fibres aid the process by providing structural support to the xerogel network during drying, as found in our previous continuous glass fibre embodiments [15] and existing, large-scale manufacture of aerogel insulation blankets using felt reinforcements [41,42].

Funding

The authors kindly acknowledge the funding for this research provided by UK Engineering and Physical Sciences Research Council (EPSRC) programme Grant EP/T011653/1, Next Generation Fibre-Reinforced Composites: a Full Scale Redesign for Compression (Next-COMP), a collaboration between Imperial College London and University of Bristol. All underlying data to support the conclusions are provided within the manuscript or ESI.

CRediT authorship contribution statement

Charles M.D. Shaw: Conceptualization, Methodology, Validation, Formal analysis, Investigation, Writing – original draft, Writing – review & editing, Visualization. **David B. Anthony:** Conceptualization, Supervision, Writing – review & editing, Project administration. **Ian Hamerton:** Conceptualization, Supervision, Writing – Review and Editing, Funding. **Milo S.P. Shaffer:** Conceptualization, Supervision, Writing – Review and Editing, Funding.

Declaration of competing interest

The authors declare that they have no known competing financial interests or personal relationships that could have appeared to influence the work reported in this paper.

Data availability

Data will be made available on request.

Acknowledgments

The authors would like to thank Daniela Wloch, Kanjanawadee Singkronart, Koon-Yang Lee, Tommaso Costantini, Samuel Baker-Humphrey, and Chris Butler for training and access to equipment at Imperial College London. This work utilised expertise and prototyping equipment at the Imperial College Advanced Hackspace.

Appendix A. Supplementary material

Supplementary data to this article can be found online at https://doi.org/10.1016/j.compositesa.2024.108164.

References

[1] Nanosilica-Toughened SS, Resins E. Polymers 2020;12(8):1777–803.
[2] Quaresimin M, Schulte K, Zappalorto M, Chandrasekaran S. Toughening mechanisms in polymer nanocomposites: From experiments to modelling. Compos Sci Technol 2016;123:187–204.
[3] Zhang H, Liu Y, Huo S, Briscoe J, Tu W, Picot OT, et al. Filtration effects of graphene nanoplatelets in resin infusion processes: problems and possible solutions. Comp Sci Tech 2017;139:138–45.
[4] Fu SY, Feng XQ, Lauke B, Mai YW. Effects of particle size, particle/matrix interface adhesion and particle loading on mechanical properties of particulate–polymer composites. Compos B: Eng 2008;39(6):933–61.
[5] Jumahat A, Soutis C, Jones FR, Hodzic A. Effect of silica nanoparticles on compressive properties of an epoxy polymer. J Mater Sci 2010;45(21):5973–83.
[6] Liu F, Deng S, Zhang J. Mechanical properties of epoxy and its carbon fiber composites modified by nanoparticles. J Nanomater 2017;1:1–9.
[7] Huang W, Shishehbor M, Guarín-Zapata N, Kirchhofer ND, Li J, Cruz L, et al. A natural impact-resistant bicontinuous composite nanoparticle coating. Nat Mater 2020;19(11):1236–43.
[8] Ching H, Thorson TJ, Paul B, Mohraz A. Rapid production of bicontinuous macroporous materials using intrinsically polymerizable bijels. Mater Adv 2021;2(15):5067–75.
[9] Liu X, Ronne A, Yu LC, Liu Y, Ge M, Lin CH, et al. Formation of three-dimensional bicontinuous structures via molten salt dealloying studied in real-time by in situ synchrotron X-ray nano-tomography. Nat Commun 2021;12(1):3441.
[10] Fang W, Mu Z, He Y, Kong K, Jiang K, Tang R, et al. Organic-inorganic covalent-ionic molecules for elastic ceramic plastic. Nature 2023;619(7969):293–9.
[11] Perchacz M, Beneš H, Zhigunov A, Serkis M, Pavlova E. Differently-catalyzed silica-based precursors as functional additives for the epoxy-based hybrid materials. Polymer 2016;99:434–46.
[12] Salimian S, Zadhoush A. Water-glass based silica aerogel: unique nanostructured filler for epoxy nanocomposites. J Porous Mater 2019;26(6):1755–65.
[13] Leventis N. Three-dimensional core-shell superstructures: mechanically strong aerogels. Acc Chem Res 2008;40(9):874–84.
[14] Lin D, Yuen PY, Liu Y, Liu W, Liu N, Dauskardt RH. A silica-aerogel-reinforced composite polymer electrolyte with high ionic conductivity and high modulus. Adv Mater 2017;30(32):1802661.
[15] Anthony DB, Nguyen S, Qian H, Xu S, Shaw CMD, Greenhalgh ES, et al. Silica aerogel infused hierarchical glass fiber polymer composites. Compos Commun 2023;39:101531.
[16] Maleki H, Durães L, Portugal A. An overview on silica aerogels synthesis and different mechanical reinforcing strategies. J Non-Cryst Solids 2014;385:55–74.
[17] Zhan W, Chen L, Kong Q, Li L, Chen M, Jiang J, et al. The synthesis and polymer-reinforced mechanical properties of SiO2 aerogels: a review. Molecules 2023;28(14):5534.
[18] Norström A, Watson H, Engström B, Rosenholm J. Treatment of E-glass fibres with acid, base and silanes. Colloids Surf A: Physicochem Eng Asp 2001;194(1–3):143–57.
[19] Zöllner M, Lieberwirth H, Kempkes P, Fendel A. Thermal resistance of carbon fibres/carbon fibre reinforced polymers under stationary atmospheric conditions and varying exposure times. Waste Manag 2019;85:327–32.
[20] Huang P-H, Laakso M, Edinger P, Hartwig O, Duesberg GS, Lai L-L, et al. Three-dimensional printing of silica glass with sub-micrometer resolution. Nat Commun 2023;14(1).
[21] Soleimani Dorcheh A, Abbasi MH. Silica aerogel; synthesis, properties and characterisation. J Mater Process Technol 2008;199:1–3.
[22] Cogan HDS, Setterstrom CA. Properties of ethyl silicate. Chem Eng News 1946;24(18):2499–501.
[23] Kajihara K. Recent advances in sol–gel synthesis of monolithic silica and silica-based glasses. J Asian Ceram Soc 2013;1(2):121–33.
[24] Bourebrab MA, Oben DT, Durand GG, Taylor PG, Bruce JI, Bassindale AR, et al. Influence of the initial chemical conditions on the rational design of silica particles. J Sol-Gel Sci Technol 2018;88(2):430–41.
[25] Woignier T, Phalippou J. Mechanical strength of silica aerogels. J Non-Cryst Solids 1988;100(1–3):404–8.
[26] Zemke F, Scoppola E, Simon U, Bekheet M, Wagermaier W, Gurlo A. Springback effect and structural features during the drying of silica aerogels tracked by in-situ synchrotron X-ray scattering. Sci Rep 2022;12(1):7537.
[27] Pisal AA, Rao AV. Comparative studies on the physical properties of TEOS, TMOS and Na2SiO3 based silica aerogels by ambient pressure drying method. J Porous Mater 2016;23(6):1547–56.
[28] Li Z, Zhao S, Koebel MM, Malfait WJ. Silica aerogels with tailored chemical functionality. Mat Des 2020;193:108833.
[29] Zhao X, Wang Y, Luo J, Wang P, Xiao P, Jiang B. The influence of water content on the growth of the hybrid-silica particles by sol-gel method. SILICON 2021;13(10):3413–21.
[30] Woignier T, Pelous J, Phalippou J, Vacher R, Courtens E. Elastic properties of silica aerogels. J Non-Cryst Solids 1987;95–96:1197–202.
[31] Nazir T, Afzal S, Siddiqi HM, Saeed S, Dumon H. The influence of temperature and interface strength on the microstructure and performance of sol–gel silica–epoxy nanocomposites. Polym Bull 2011;67(8):1539–51.
[32] Horbach J, Kob W, Binder K. Specific heat of amorphous silica within the harmonic approximation. J Phys Chem B 1999;103(20):4104–8.

[33] Shaw C M D, Anthony A B, Hamerton I, Shaffer M S P. Bicontinuous Silica-Epoxy Nanocomposites. In: Proceedings of ICCM 23 Conference, Belfast, August, 2023, Paper 349, 9 pages. <https://iccm-central.org/Proceedings/ICCM23proceedings/papers/ICCM23_Full_Paper_349.pdf>.
[34] Smirnov S, Konovalov D, Veretennikova I, Pestov A, Smirnova E. Effect of modifying dopes on the mechanical properties of epoxy coatings affected by thermocycling. Procedia Struct Integr 2020;25:209–13.
[35] Oliver WC, Pharr GM. An improved technique for determining hardness and elastic modulus using load and displacement sensing indentation experiments. J Mater Res 1992;7(6):1564–83.
[36] Ma HS, Roberts AP, Prévost JH, Jullien R, Scherer G. Mechanical structure-property relationship of aerogels. J Non-Cryst Solids 2000;277(2–3):127–41.
[37] Moner-Girona M, Roig A, Molins E, Martínez E, Esteve J. Micromechanical properties of silica aerogels. Appl Phys Lett 1999;75(5):653–5.
[38] Tzetzis D, Mansour G. Nanoindentation, compression and fractural characterization of highly dispersed epoxy-silica nanocomposites. J Reinf Plast Compos 2016;35(7):541–55.
[39] Johnsen BB, Kinloch AJ, Mohammed RD, Taylor AC, Sprenger S. Toughening mechanisms of nanoparticle-modified epoxy polymers. Polymer 2007;48:530–41.
[40] Ma J, Mo M-S, Du X-S, Rosso P, Friedrich K-C. Effect of inorganic nanoparticles on mechanical property, fracture toughness and toughening mechanism of two epoxy systems. Polymer 2008;49:3510–23.
[41] Sharma J, Sheikh J, Behera BK. Aerogel composites and blankets with embedded fibrous material by ambient drying: Reviewing their production, characteristics, and potential applications. Dry Technol 2023;41(6):915–47.
[42] Parmenter KE, Milstein F. Mechanical properties of silica aerogels. J Non-Cryst Solids 1998;223(3):179–89.